Electronic Supporting Information

Interface Engineering of Hierarchical NiCoP/$NiCoS_x$ Heterostructure Arrays for Efficient Alkaline Hydrogen Evolution at Large Current Density

Weiwei Han, [a] Fan Zhang,[a] Lingshu Qiu,[a] Yang Qian,[a] Shaoyun Hao,[a] Ping Li, [b] Yi He,[a] Xingwang Zhang, *[ab]

a. Key Laboratory of Biomass Chemical Engineering of Ministry of Education, College of Chemical and Biological Engineering, Zhejiang University, Hangzhou, Zhejiang Province 310027, China.
b. Institute of Zhejiang University-Quzhou, Quzhou, Zhejiang Province 324000, China.

*Corresponding author E-mail: xwzhang@zju.edu.cn

1. Experimental section

1.1 Materials and chemicals

Nickel (Ⅱ) chloride hexahydrate ($NiCl_2·6H_2O$, 98.0%), cobalt (Ⅱ) chloride hexahydrate ($CoCl_2·6H_2O$, AR), thiourea (CH_4N_2S, 99.0%), sodium hypophosphite (NaH_2PO_2, 99.0%), sodium citrate dihydrate ($C_6H_5Na_3O_7·2H_2O$, 99.0%) were purchased from Aladdin Reagent (Shanghai) Co., Ltd. Potassium hydroxide (KOH, 85.0%), hydrochloric acid (HCl, 36–38%), ethanol and acetone were purchased from Sinopharm Chemical Reagent Co., Ltd. Commercial Pt/C (20 wt%) was purchased from Macklin Biochemical Technology Co., Ltd. Nafion solution (5 wt%) was bought from Du Pont Company. Ni foam (thickness: 1 mm, porosity: ca. 95%) was bought from Jiashide Foam Metal Co., Ltd (Suzhou, China). Ultrapure Milli-Q water (18.2 MΩ cm^{-1}) was used for all experiments.

1.2 Materials synthesis

1.2.1 Synthesis of $NiCoS_x$/NF

Prior to preparation, Ni foam (NF) was cut into small pieces (1.0 × 1.5 cm). Then the pieces were cleaned ultrasonically several times in acetone, HCl (3 M), ethanol and ultrapure water followed by vacuum drying overnight at 40 ℃. $NiCoS_x$/NF was prepared using a cyclic voltammetry (CV) electrodeposition method in a three-electrode cell. NF, Pt plate and saturated calomel electrode (SCE) were used as the working electrode, counter electrode and reference electrode, respectively. 40 mL of solution containing 0.05 M $NiCl_2·6H_2O$, 0.125 M $CoCl_2·6H_2O$ and 0.5 M CH_4N_2S were used as electrolyte. CV was performed in the range of −1.3~0.3 V vs. SCE at a scan rate of 5 mV s^{-1} for 4 cycles under stirring. Subsequently, the obtained electrode was rinsed with ultrapure water and dried at 40 ℃ in a vacuum oven. The NiS_x/NF was synthesized using the same method without the addition of $CoCl_2·6H_2O$ in the electrolyte. In addition, the optimization of catalyst electrodeposition conditions was design by single variable method as shown in the **Table S1**–**S3**.

1.2.2 Synthesis of NiCoP/$NiCoS_x$/NF

The nickel-cobalt phosphide (NiCoP) layer was then coated on the surface of $NiCoS_x$/NF by electrodeposition, too. The electrolyte contained 55 mM $CoCl_2·6H_2O$, 33 mM $NiCl_2·6H_2O$, 20 mM $C_6H_5Na_3O_7·2H_2O$ and 0.2 M NaH_2PO_2. The graphite rod and Ag/AgCl electrode were employed as the counter electrode and reference electrode, respectively. The electrodeposition process was

carried out at a constant potential of –1.2 V vs. Ag/AgCl for 25 min, then the obtained electrode was rinsed with ultrapure water and dried in vacuum at 40 ℃. In order to determine optimal deposition time, a series of CoP/NiS_x/NF were prepared by applying different electrodeposition time. In addition, CoP/NF, NiCoP/NF, CoP/$NiCoS_x$/NF were also prepared without the addition of corresponding precursors under the same depositional conditions. The masses of loaded catalysts on NF are about 2.0, and 5.8 mg cm^{-2} for $NiCoS_x$/NF and NiCoP/$NiCoS_x$/NF, respectively.

1.3 Materials characterization

The crystalline structures of samples were characterized by X-ray diffractometer (XRD, PANalytical B.V. X-pert Powder, Cu Ka = 1.5406 Å). Scanning electron microscopy (SEM, Hitachi SU-70) and transmission electron microscope (TEM, FEI Tecnai G2 F20 S-TWIN) equipped with energy dispersive X-Ray spectrometer (EDX) were used to characterize the morphology. Raman spectra was conducted on a LabRAM HR Evolution spectrometer combined with a 633 nm excitation laser. The valence states and binding energy of materials were obtained by X-ray photoelectron spectrometer (XPS, Thermo Scientific K-Alpha) with an Al Kα excitation source. The contact angle (CA) measurements were performed by LAUDA OSA200-T.

1.4 Electrochemical Measurements

Electrochemical measurements were carried out using a standard three-electrode system on a Bio-Logic VSP potentiostat with 1 M KOH as the electrolyte. The as-prepared materials (1.0 × 0.7 cm) were employed as the working electrodes, while graphite rod and Hg/HgO electrode were used as the counter electrode and reference electrode, respectively. Unless otherwise stated, all the potentials with *iR* compensation were referred to the reversible hydrogen electrode (RHE) by the Nernst equation unless otherwise stated:

$$E_{RHE} = E_{Hg/HgO} + 0.098\ V + 0.0591 \times pH \quad (S1)$$

The linear sweep voltammetry (LSV) measurements were conducted at a scan rate of 5 mV s^{-1}. The electrochemical impedance spectroscopy (EIS) was recorded at –1.1 V vs. Hg/HgO in a frequency range of 100 kHz to 0.01 Hz with an amplitude of 5 mV. The uncompensated resistance (*R*) was determined by fitting the EIS data to an equivalent electrical circuit. Double-layer capacitances (C_{dl}) could be assessed by cyclic voltammetry (CV) from 0.1 to 0.2 V vs. RHE with different scan rates ranging from 20 to 140 mV s^{-1}. The long-term stability was investigated by chronopotentiometry

(CP) measurements and CV at a scan rate of 100 mV s^{-1}. Moreover, the commercial Pt/C was deposited on Ni foam as the comparative electrode. Specially, 10 mg Pt/C (20 wt%) and 10 μL of Nafion solution (5 wt%) was dispersed in 1 ml mixture of ethanol and water (1: 3, *v*: *v*) under the ultrasonic wave. Then 200 μL of ink was coated on Ni foam followed by drying at room temperature.

1.5 Theoretical calculations

The density functional theory (DFT) calculations were performed using Vienna ab initio simulation package (VASP)[1-3] within periodic models. Generalized gradient approximation (GGA) with projector augmented wave (PAW) method was applied in calculations to simulate the electronic structures and the core-electron interaction. The energy cutoff was set to be 450 eV. The spin polarization effect was considered in this work, and the initial magnetic moments of Ni and Co were set to 5. To improve the description of the d electrons, here the Hubbard DFT+U method was employed. The effective U values for Ni and Co d orbitals were 3.4 and 6 eV, respectively.[4] Structural optimizations were performed until the residual forces on each ion converged to smaller than 0.05 eV $Å^{-1}$. To simplify the calculation, $NiCo_2S_4$ was chose in place of $NiCoS_x$. The lattice parameters of NiCoP and $NiCo_2S_4$ were optimized by 8×8×12 and 5×5×5 k-meshes, respectively. Using the optimized lattice parameters, six-layer NiCoP (001) and twelve-layer $NiCo_2S_4$ (111) facets were built. The bottom half layers were fixed while the other atoms were fully relaxed during all of the calculations involving the two surfaces. The 2×2×1 k-meshes were utilized to describe the surface Brillouin zone. The NiCoP/$NiCo_2S_4$ heterojunction were built by combing the NiCoP (001) and $NiCo_2S_4$ (111) facets. The width of vacuum layer for all the surface structures and heterojunction was set larger than 12 Å to avoid spurious interaction. The adsorption energy of H species on the considered slabs is defined as:

$$\Delta E_H = E_{slab+H} - E_{slab} - 0.5E_{H_2(g)} \quad \text{(S2)}$$

where E_{slab+H} means the total energy of slab and adsorbed atomic H, E_{slab} denotes the slab energy and $E_{H_2(g)}$ represents the energy of the H_2 species in gas phase. The entropy (*TS*) and zero-point energy (E_{ZPE}) are also involved in calculations to obtain the Gibbs free adsorption energy of adsorbed atomic H:

$$\Delta G_H = \Delta E_H + \Delta E_{ZPE} - T\Delta S \quad \text{(S3)}$$

2. Supplementary calculation methods.

2.1 Calculation of electrochemical active surface area.

The electrochemical active surface area (ECSA) can be estimated from the electrochemical double-layer capacitance (C_{dl}) of the catalysts by the following equation:

$$\mathrm{ECSA} = \frac{C_{dl}}{C_s} \tag{S4}$$

where C_s is the specific capacitance for a flat surface ranging between 20 and 60 μF cm^{-2}, and it was assumed as the average value of 40 μF cm^{-2} in this work.

The C_{dl} values can be derived from the CV curves in **Figure S7**, according to the equation below:

$$\Delta j/2 = v \times C_{dl} \tag{S5}$$

where Δj corresponds to the difference between anodic and cathodic current density ($j_{anode} - j_{cathode}$) at 0.15 V vs. RHE, v is the corresponding scan rate. The fitted slope of the curve ($\Delta j/2$ against v) is equal to the C_{dl} value.

2.2 Calculation of turnover frequency.

The turnover frequency (TOF) for HER were calculated on the hypothesis that all the active sites were involved in the electrocatalytic process based on previous reports.

$$\mathrm{TOF} = \frac{\#\text{total } H_2 \text{ turn overs/cm}^2 \text{ geometric area}}{\#\text{surface sites/cm}^2 \text{ geometric area}} \tag{S6}$$

The total number of H_2 turn overs was determined by the current density from the LSV curves using the following equation:

$$\#_{H_2} = (j\frac{\mathrm{mA}}{\mathrm{cm}^2})(\frac{1\ \mathrm{C\ s^{-1}}}{1000\ \mathrm{mA}})(\frac{1\ \mathrm{mol\ e^-}}{96485\ \mathrm{C}})(\frac{1\ \mathrm{mol\ H_2}}{2\ \mathrm{mol\ e^-}})(\frac{6.022\times10^{23}\ \mathrm{mol\ H_2}}{1\ \mathrm{mol\ H_2}})$$

$$= 3.12\times10^{15}\frac{\mathrm{H_2/s}}{\mathrm{cm}^2}\ \mathrm{per}\ \frac{\mathrm{mA}}{\mathrm{cm}^2} \tag{S7}$$

The number of effective surface sites was calculated based on the following equation:

$$\frac{\#\text{surface sites}}{\mathrm{cm}^2 \text{ geometric area}} = \frac{\#\text{active sites(flat standard)}}{\mathrm{cm}^2 \text{ geometric area}} \times \text{Roughness factor} \tag{S8}$$

Where the roughness factor is determined by A_{ECSA}, and the number of the surface active sites per real surface area is demonstrated by the following calculation formula:

$$\#\text{active sites} = \left(\frac{\text{number of atoms per unit cell}}{\text{unit cell volume}}\right)^{\frac{2}{3}} \quad \text{(S9)}$$

Here, since the exact hydrogen binding sites were unclear, we conservatively took the number of active sites for $NiCoP/NiCoS_x$ was about 1.1573×10^{15} atoms cm_{real}^{-2} which was deduced from the average value of NiCoP (1.707×10^{15} atoms cm_{real}^{-2}) and $NiCo_2S_4$ (6.076×10^{14} atoms cm_{real}^{-2}).

As a result, LSV plot can be converted into a TOF plot through the following formula:

$$\text{TOF} = \frac{\left(3.12 \times 10^{15} \frac{H_2/s}{cm^2} \text{ per } \frac{mA}{cm^2}\right) \times |j|}{\#\text{active sites} \times A_{ECSA}} \quad \text{(S10)}$$

2.3 Calculation of Faradaic efficiency.

To calculate the Faradaic efficiency (FE) of HER, chronopotentiometry was conducted at 100 mA in the H-type electrolytic cell. The evolved H_2 volume was measured by water drainage method synchronously. The FE can be calculated with the following equation:

$$FE\% = \frac{znF}{Q} \times 100\% \quad \text{(S11)}$$

where z, *n*, *F* and *Q* represent the number of electrons transferred for a hydrogen molecule, moles of produced H_2 measured from the volume of H_2, the Faraday constant (96485 C mol^{-1}) and the total electric quantity applied, respectively.

Table S1. The influence of deposition cycles on NiS_x/NF catalytic performance.

Ni^{2+} (mol L^{-1})	CH_4N_2S (mol L^{-1})	Deposition cycles
0.05	0.75	1
		4
		7
		10

Table S2. The influence of the concentration of thiourea on NiS_x/NF catalytic performance.

Ni^{2+} (mol L^{-1})	CH_4N_2S (mol L^{-1})	Deposition cycles
0.05	0.25	4
	0.5	
	0.75	
	1	

Table S3. The influence of molar ratio of Co^{2+}/Ni^{2+} on $NiCoS_x$/NF catalytic performance.

Ni^{2+} (mol L^{-1})	Co^{2+}/Ni^{2+} molar ratio	CH_4N_2S (mol L^{-1})	Deposition cycles
0.05	1:1	0.5	4
	2:1		
	5:2		
	3:1		

Table S4. Comparison of HER performance of NiCoP/$NiCoS_x$/NF with other recently reported HER electrocatalysts in 1 M KOH.

Electrode	**η_{10} (mV)**	**η_{100} (mV)**	**η_{500} (mV)**	**Tafel slope (mV dec^{-1})**	**Stability (h) @ j or E**	**Reference**
NiCoP/$NiCoS_x$/NF	**68**	**144**	**222**	**59**	**110@500 mA cm^{-2}**	**This work**
$PB_{0.94}$C-DSPH/GCE	186	NA	364	56.5	10@500 mA cm^{-2}	*Small Methods,* **2021**, *5,* 2000701
Fe-Mo-S/Ni_3S_2@NF	141	266	384	123	24@160 mA cm^{-2}	*Chem. Eng. J.,* **2021**, *404,* 126483
V-FeP/IF(Iron foam)	NA	149	246	40.97	24@500 mA cm^{-2}	*J Colloid Interface Sci*, **2022**, *615*, 445-455
Co_2P-Co_3O_4/Ti plate	86	275	NA	73	90@500 mA cm^{-2}	*Adv. Energy Mater.*, **2018**, *8*, 1802445
$MoSe_2$-Mo_2N/Mo	76	NA	<400	69.5	30@–0.12 V	*J. Mater. Chem. A*, **2021**, *9*, 26113−26118
$Ni_{11}(HPO_3)_8(OH)_6$/NF	121	271	>350	102	24@–0.13 V	*Energy Environ. Sci.*, **2018**, *11*, 1287−1298
F-Co_2P/Fe_2P/IF	NA	151.8	229.8	115.01	10@500 mA cm^{-2}	*Chem. Eng. J.,* **2020**, *399,* 125831
Ni NWs/E-Ni mesh	87	169	204	75	100@500 mA cm^{-2}	*J. Power Sources*, **2021**, *516*, 230635
P-Ni_2P/NF	134	246	420	92	48@500 mA cm^{-2}	*Int. J. Hydrog. Energy*, **2019**, *44*, 5739−5747
$Ni_{2(1-x)}Mo_{2x}P$/NF	72	162	240	46.4	100@–	*Nano Energy*, **2018**,

					0.11 V	*53*, 492−500
$CoMoS_x$/NF	89	NA	269	94	25@500 mA cm^{-2}	*Angew Chem Int Ed Engl,* **2020,** *59*, 1659-1665
$F_{0.25}C_1CH$/NF	77	180	246	99	136@100 mA cm^{-2}	*Adv. Energy Mater.*, **2018**, *8*, 1800175
3F-FeP/IF(Iron foam)	NA	191	261	56.12	24	*Fuel*, **2022**, *316*, 123206
F, P-Fe_3O_4/IF	NA	179.5	277.6	127.9	12@500 mA cm^{-2}	*J. Mater. Chem. A,* **2021,** *9*, 15836-15845

Table S5. Resistance values of different catalysts obtained from fitting electrical equivalent circuit model.

Sample	NF	$NiCoS_x$/NF	NiCoP/NF	NiCoP/$NiCoS_x$/NF	Pt/C on NF
R_s (Ω)	2.022	1.712	1.431	1.375	1.366
R_{ct} (Ω)	47.84	29.16	8.562	0.8955	0.3586

Table S6. Data of d-band centers (ε_d).

Sample	ε_d up	ε_d down	Average ε_d
NiCoP	-3.06	-2.74	-2.90
$NiCo_2S_4$	-3.69	-2.93	-3.31
NiCoP/$NiCo_2S_4$	-2.83	-2.73	-2.78

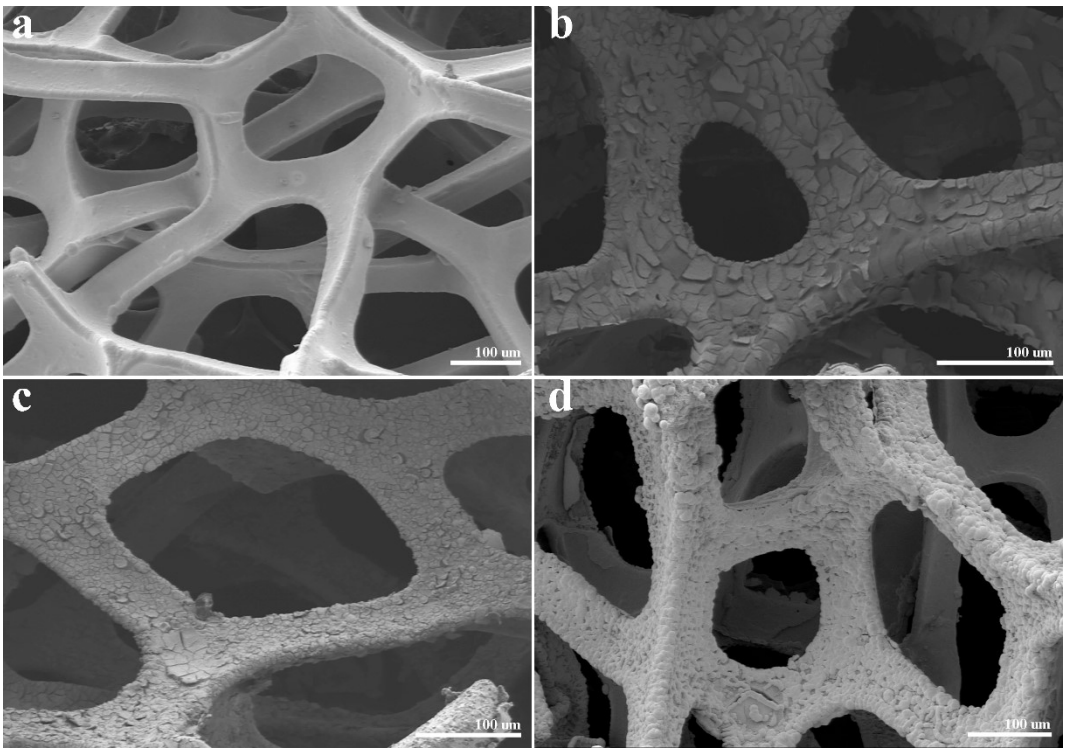

Figure S1. SEM images of (a) NF, (b) NiS_x/NF, (c) $NiCoS_x$/NF and (d) NiCoP/$NiCoS_x$/NF.

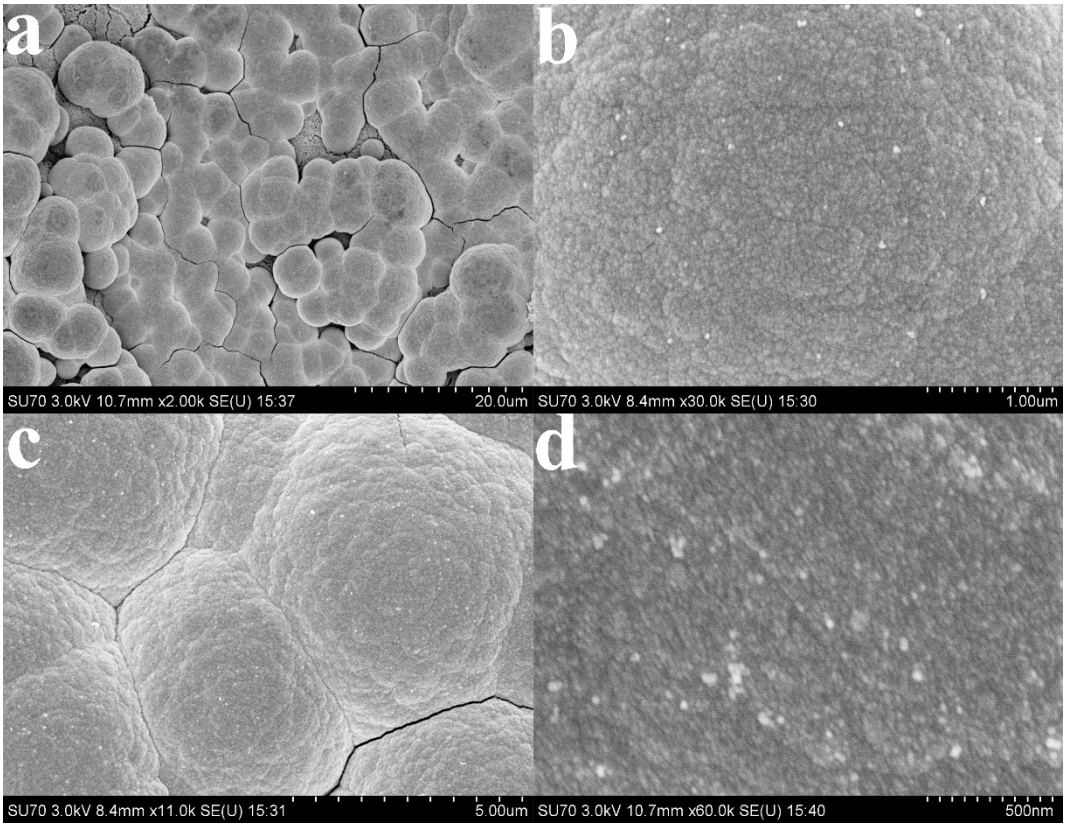

Figure S2. Different magnification of SEM images for NiCoP/$NiCoS_x$/NF.

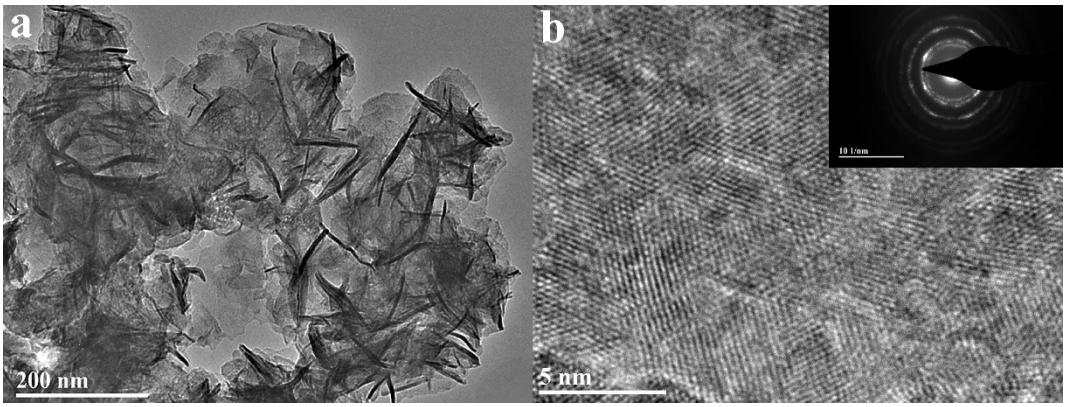

Figure S3. (a) TEM image and (b) HRTEM image of NiCoP/$NiCoS_x$/NF (the inset of (b) shows the SAED pattern of NiCoP/$NiCoS_x$/NF).

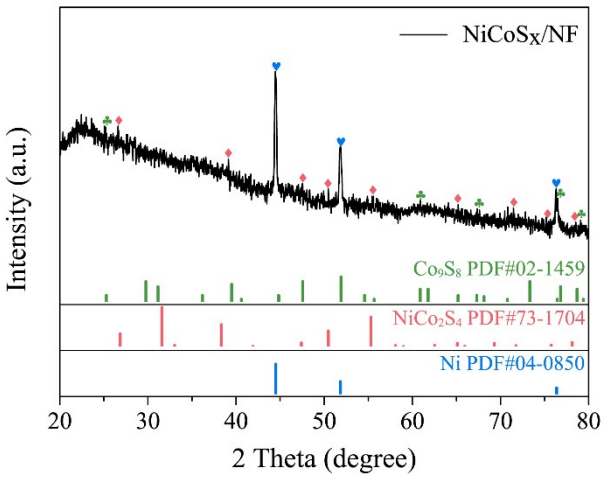

Figure S4. XRD pattern of $NiCoS_x$/NF.

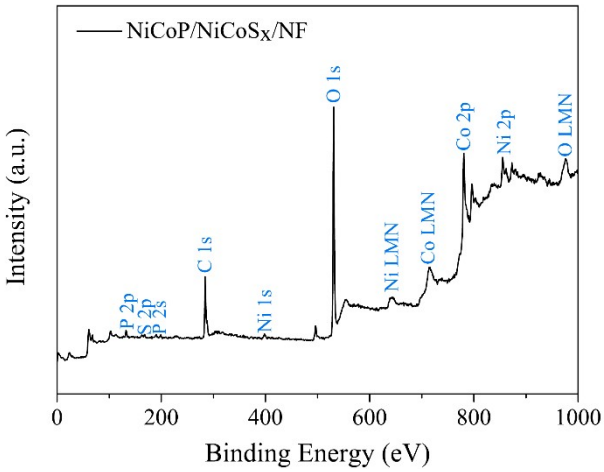

Figure S5. XPS survey spectra of NiCoP/$NiCoS_x$/NF.

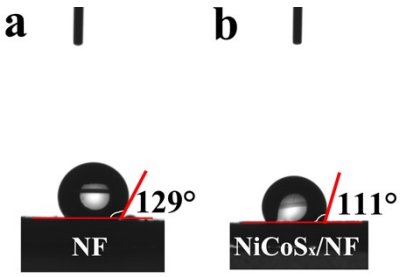

Figure S6. Contact angle images of (a) NF and (b) $NiCoS_x$/NF.

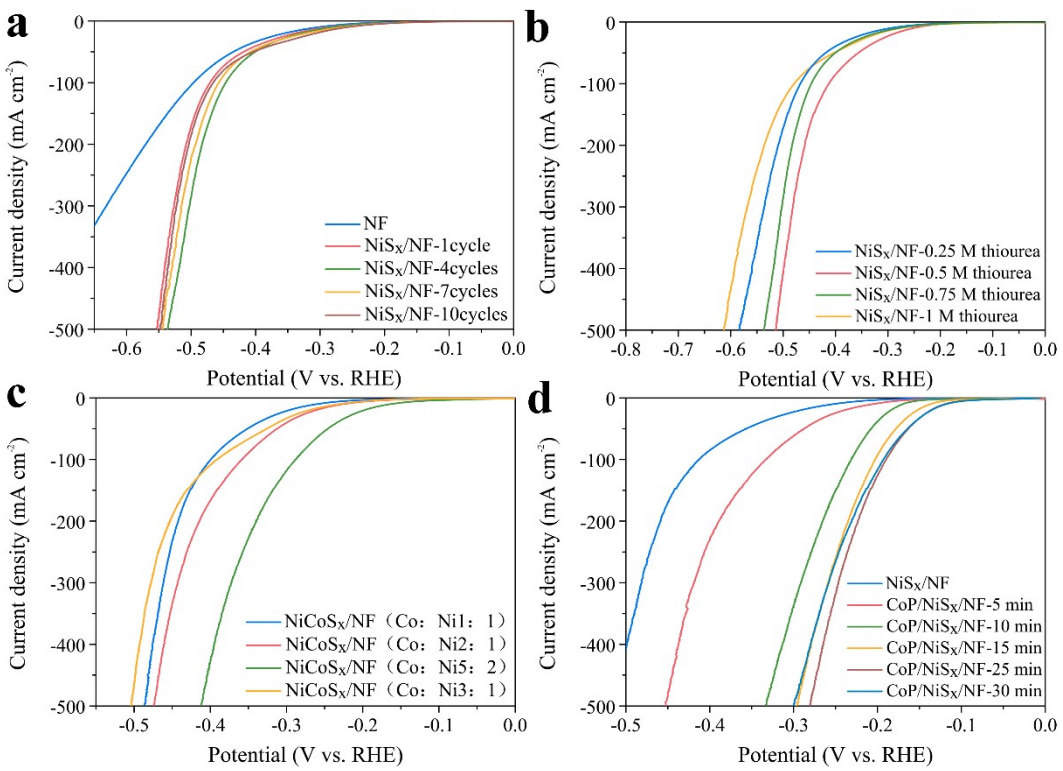

Figure S7. HER polarization curves of NiS_x/NF deposited with (a) different cycles and (b) different concentration of thiourea, (c) polarization curves of $NiCoS_x$/NF deposited under different Co/Ni molar ratio, (d) polarization curves of CoP/NiS_x/NF obtained under different electrodeposition time.

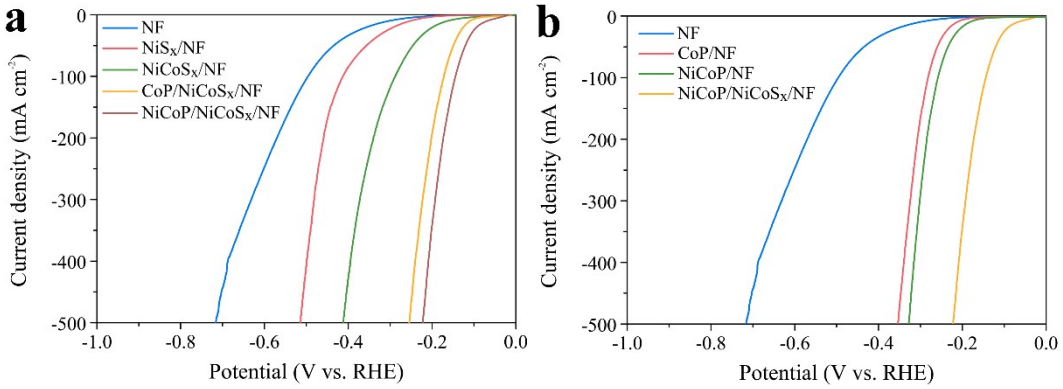

Figure S8. Comparison of HER polarization curves (a) based on sulfides and (b) based on phosphides.

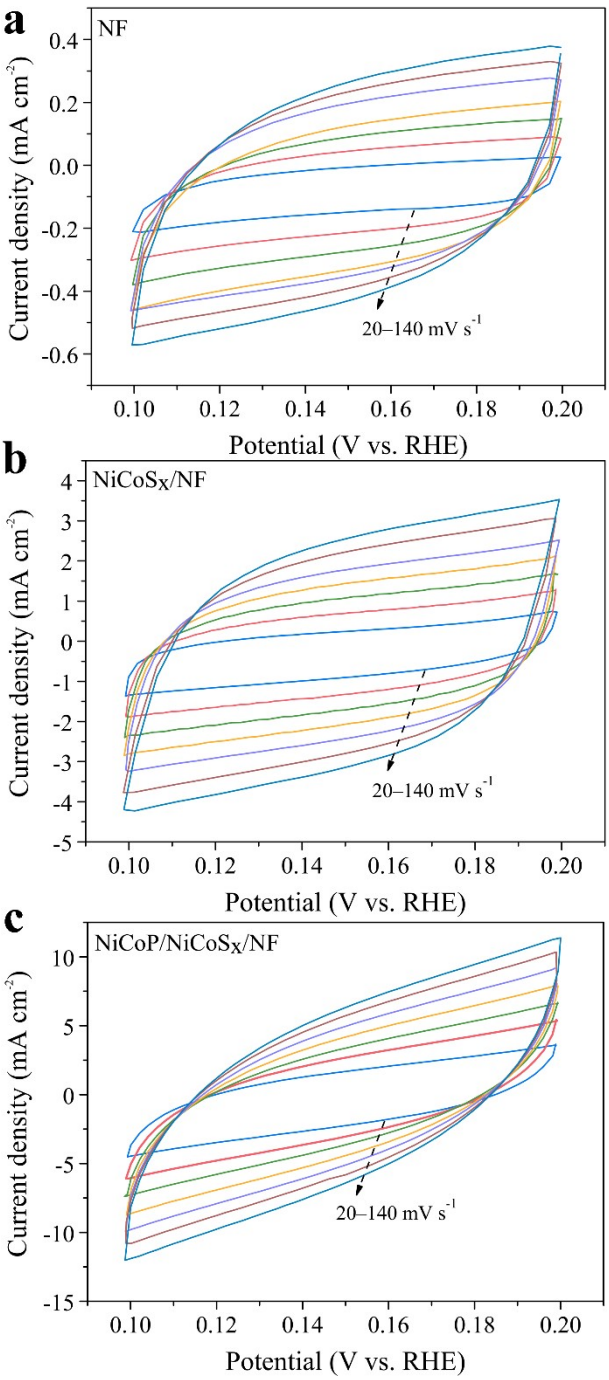

Figure S9. CV curves of (a) NF, (b) $NiCoS_x$/NF and (c) NiCoP/$NiCoS_x$/NF at different scan rates in the potential range of 0.1–0.2 V vs. RHE.

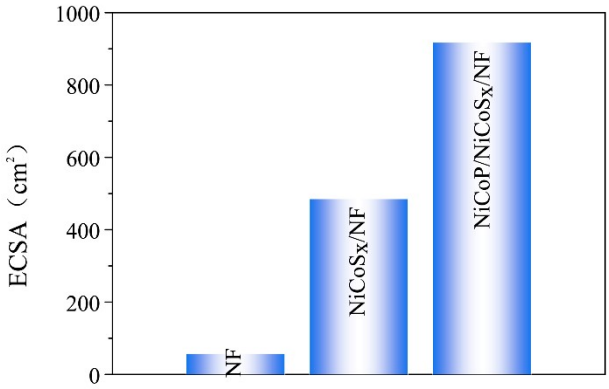

Figure S10. The ECSA values of NF, $NiCoS_x$/NF, and NiCoP/$NiCoS_x$/NF for HER.

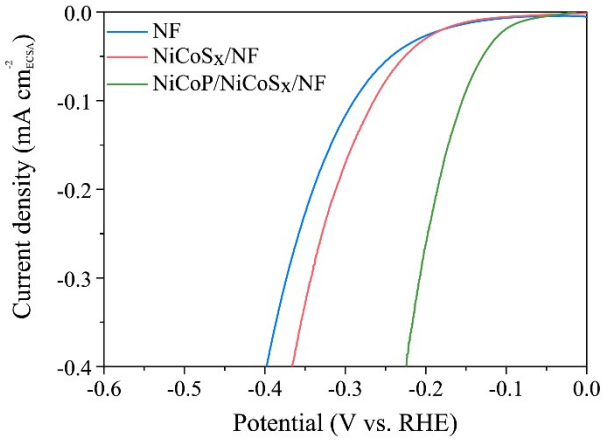

Figure S11. ECSA-normalized polarization curves of NF, $NiCoS_x$/NF and NiCoP/$NiCoS_x$/NF for HER in 1 M KOH.

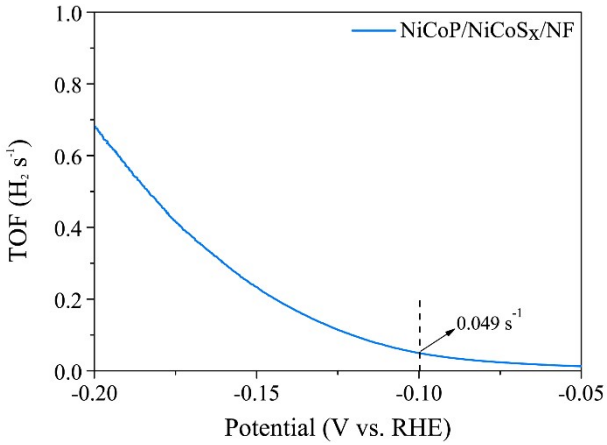

Figure S12. Calculated TOF values of NiCoP/$NiCoS_x$/NF electrode for HER.

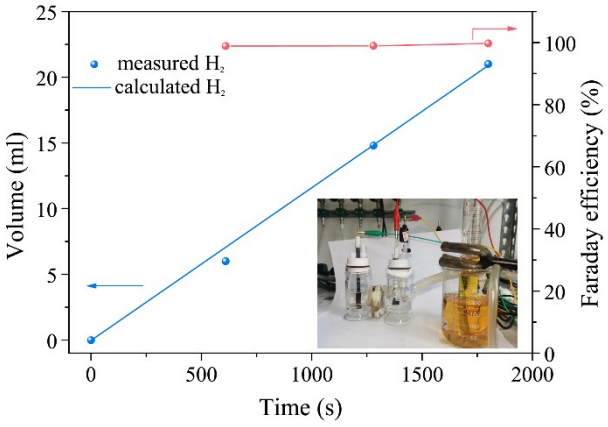

Figure S13. Volume of produced H_2 as a function of time and corresponding Faradaic efficiency during HER test at current of 100 mA (Inset: a photograph of the gas collection device).

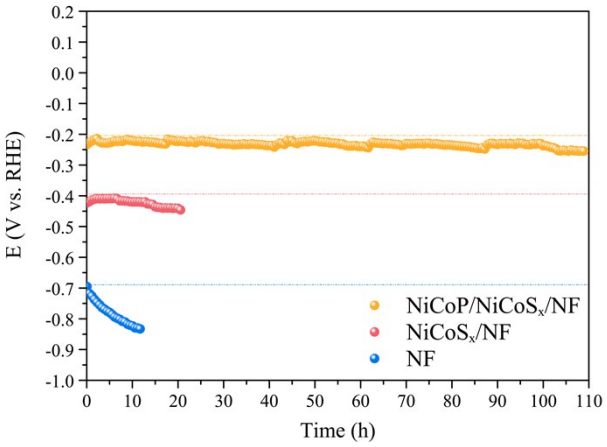

Figure S14. Chronopotentiometry curves of NF, $NiCoS_x$/NF and NiCoP/$NiCoS_x$/NF electrode recorded at 500 mA cm^{-2} in 1 M KOH.

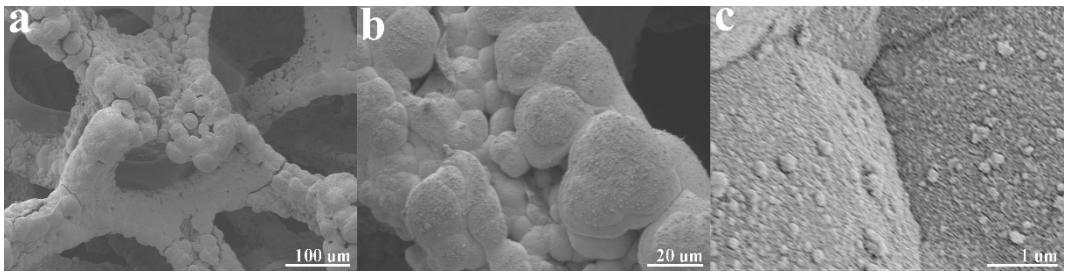

Figure S15. SEM images of NiCoP/$NiCoS_x$/NF after HER stability test.

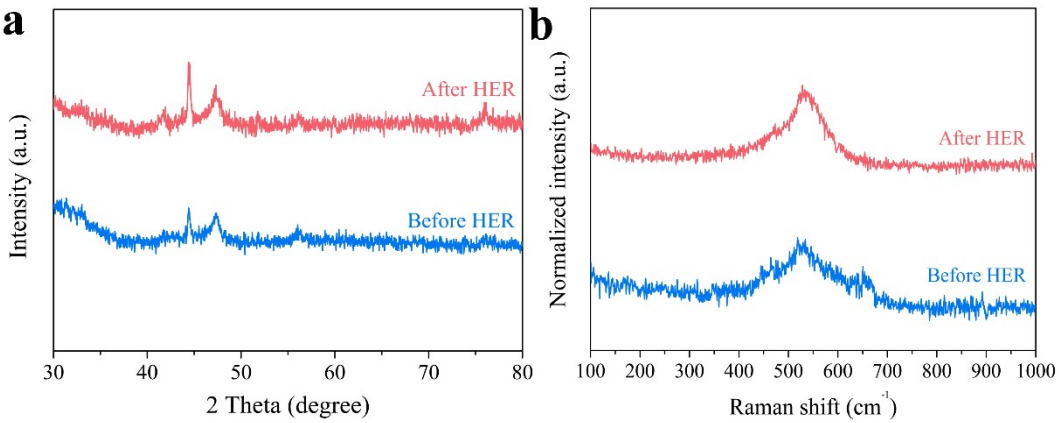

Figure S16. **(a)** XRD pattern **(b)** Raman spectra of NiCoP/NiCoS$_x$/NF before and after HER stability test.

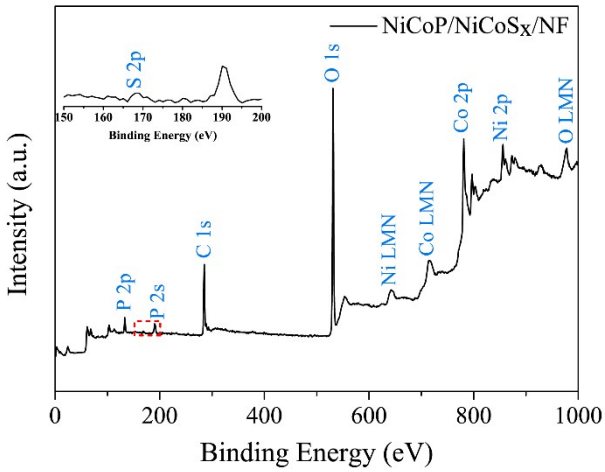

Figure S17. XPS survey spectra of NiCoP/NiCoS$_x$/NF after HER stability test and the amplified spectrum of S2p (inset).

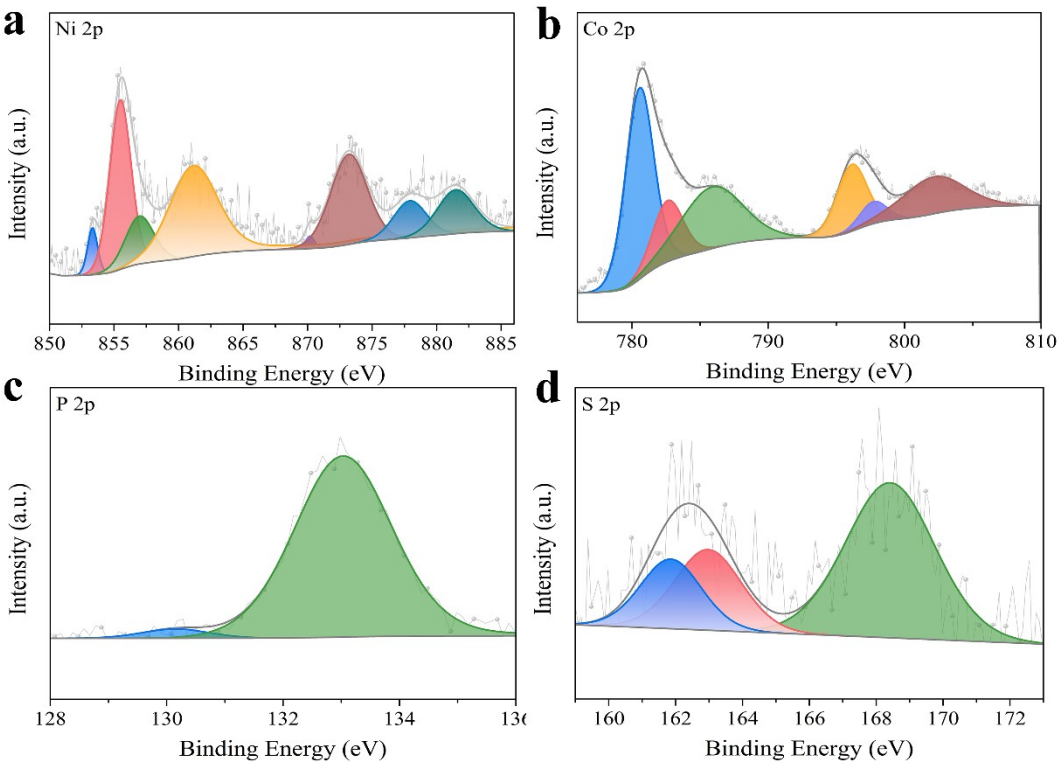

Figure S18. High-resolution XPS spectra of NiCoP/NiCoS$_x$/NF after HER stability test: (a) Ni 2p, (b) Co 2p, (c) P 2p and (d) S 2p.

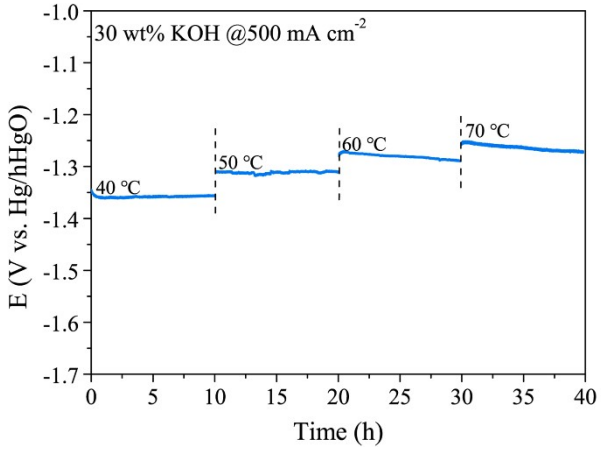

Figure S19. Chronopotentiometry curves without *iR* compensation of NiCoP/NiCoS$_x$/NF electrode operated at different temperatures at 500 mA cm^{-2} in 30% KOH solution.

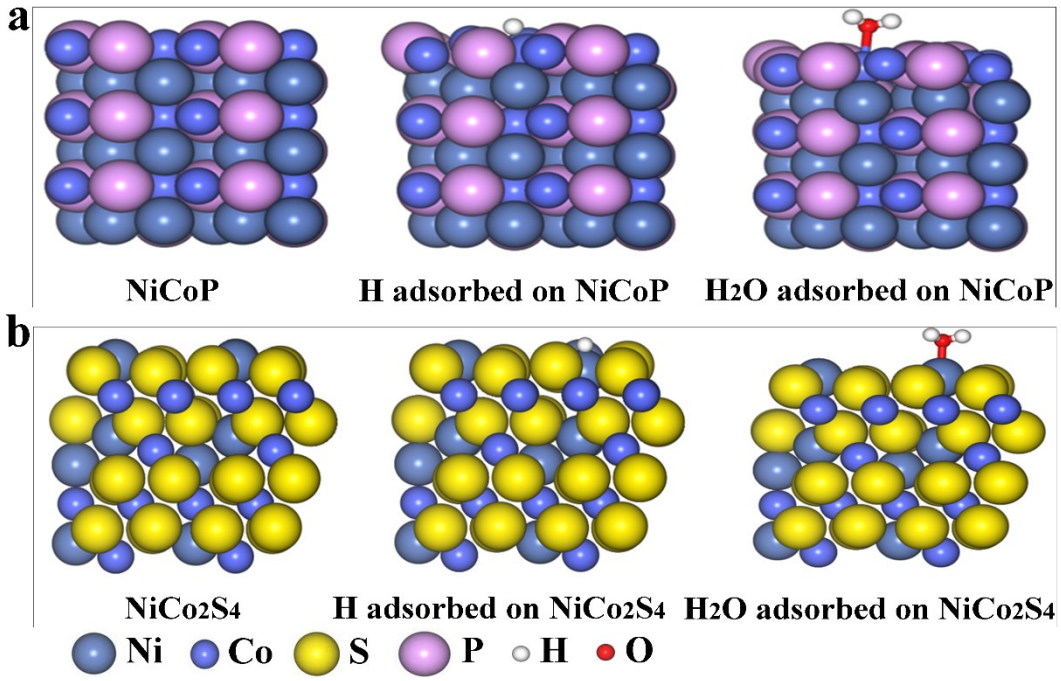

Figure S20. The optimized structure models for adsorption of intermediates (H^* and H_2O^*) on the (a) $NiCo_2S_4$ and (b) NiCoP, in which the indigo, blue, yellow, purple, white and red spheres refer to Ni, Co, S, P, H and O, respectively.

References

1. G. Kresse and J. Hafner, *Phys. Rev. B*, 1993, **47**, 558-561.
2. G. Kresse and J. Hafner, *Phys. Rev. B*, 1994, **49**, 14251-14269.
3. G. Kresse and J. Furthmüller, *Phys. Rev. B*, 1996, **54**, 11169-11186.
4. A. Jain, G. Hautier, C. J. Moore, S. Ping Ong, C. C. Fischer, T. Mueller, K. A. Persson and G. Ceder, *Comput. Mater. Sci.*, 2011, **50**, 2295-2310.